Control Engineering Practice 85 (2019) 246–256

Contents lists available at ScienceDirect

Control Engineering Practice

journal homepage: www.elsevier.com/locate/conengprac

Robust path-following control for articulated heavy-duty vehicles

Filipe Marques Barbosa [a], Lucas Barbosa Marcos [a], Maíra Martins da Silva [b], Marco Henrique Terra [a], Valdir Grassi Junior [a,*]

[a] Department of Electrical and Computer Engineering, São Carlos School of Engineering, University of São Paulo, São Carlos, Brazil
[b] Department of Mechanical Engineering, São Carlos School of Engineering, University of São Paulo, São Carlos, Brazil

ARTICLE INFO

Keywords:
Articulated vehicle
Path following
Lateral control
Robust control
Heavy-duty vehicle

ABSTRACT

Path following and lateral stability are crucial issues for autonomous vehicles. Moreover, these problems increase in complexity when handling articulated heavy-duty vehicles due to their poor manoeuvrability, large sizes and mass variation. In addition, uncertainties on mass may have the potential to significantly decrease the performance of the system, even to the point of destabilising it. These parametric variations must be taken into account during the design of the controller. However, robust control techniques usually require offline adjustment of auxiliary tuning parameters, which is not practical, leading to sub-optimal operation. Hence, this paper presents an approach to path-following and lateral control for autonomous articulated heavy-duty vehicles subject to parametric uncertainties by using a robust recursive regulator. The main advantage of the proposed controller is that it does not depend on the offline adjustment of tuning parameters. Parametric uncertainties were assumed to be on the payload, and an $\mathcal{H}_\infty$ controller was used for performance comparison. The performance of both controllers is evaluated in a double lane-change manoeuvre. Simulation results showed that the proposed method had better performance in terms of robustness, lateral stability, driving smoothness and safety, which demonstrates that it is a very promising control technique for practical applications.

1. Introduction

The advantages of autonomous vehicles are well-established in the academic literature. For example, reducing the number of accidents; easing the transportation of elderly and disabled people (Wu et al., 2015); offering more profitable means of transportation to industries and more efficient transportation methods to the military (Fu, Zhang, Yang, Zhu, & Wang, 2015; Shin, Huh, & Park, 2015); improving ride comfort for passengers (Massera Filho, Terra, & Wolf, 2017); increasing road utilisation (Dias, Pereira, & Palhares, 2014), etc.

Nowadays, heavy load vehicles are responsible for much of cargo transportation. The use of articulated heavy vehicles has been increasing due to their economic advantages (Kati, Köroğlu, & Fredriksson, 2016), freight transportation efficiency (Jujnovich & Cebon, 2013) and the growing demand for high capacity transport vehicles (Islam, Laine, & Jacobson, 2015). Furthermore, the same technologies used for autonomous cars can also be addressed to articulated heavy-duty vehicles (Fagnant & Kockelman, 2015), additionally increasing productivity and reducing cargo transportation costs (Noorvand, Karnati, & Underwood, 2017).

In the literature, different control techniques have been used to solve the path-following problem for autonomous vehicles. Alcala, Puig, Quevedo, Escobet, and Comasolivas (2018) used a Lyapunov-based technique with linear quadratic regulator-linear matrix inequality (LQR-LMI) tuning to solve the problem of guidance in an autonomous vehicle. Ji, He, Lv, Liu, and Wu (2018) proposed a robust steering controller based on a backstepping variable structured control to maintain the yaw stability and minimise the lateral error. Matraji, Al-Durra, Haryono, Al-Wahedi, and Abou-Khousa (2018) designed and implemented an adaptive Second Order Sliding Mode Control for a four wheels Skid-Steered Mobile Robot. The objective was to follow a predefined trajectory in the presence of disturbance and parametric uncertainties. Chu, Sun, Wu, and Sepehri (2018) applied an active disturbance rejection control to a steering controller design with the aim to guarantee the lane keeping of the vehicle in the presence of uncertainties and external disturbance. Lastly, Hu, Jing, Wang, Yan, and Chadli (2016) presented an $\mathcal{H}_\infty$ output-feedback control strategy based on the mixed genetic algorithms and linear matrix inequalities to perform the path following of autonomous ground vehicles.

In addition, some authors have proposed the use of an active trailer steering system to improve path following and attitude control of articulated vehicles (Guan, Kim, & Wang, 2017; Jujnovich & Cebon, 2013; Kim, Guan, Wang, Guo, & Liang, 2016). For instance, different

* Correspondence to: Department of Electrical and Computer Engineering, São Carlos School of Engineering, University of São Paulo, Av. Trabalhador São-carlense 400, 13566-590, São Carlos, SP, Brazil.
E-mail addresses: marquesfilipeb@usp.br (F.M. Barbosa), lucasbmarcos@usp.br (L.B. Marcos), mairams@sc.usp.br (M.M. da Silva), terra@sc.usp.br (M.H. Terra), vgrassi@usp.br (V. Grassi Junior).

https://doi.org/10.1016/j.conengprac.2019.01.017
Received 25 July 2018; Received in revised form 26 November 2018; Accepted 29 January 2019
Available online 22 February 2019
0967-0661/

vehicle conditions have been considered by Guan et al. (2017) for deriving a model predictive control strategy. Regarding autonomous articulated vehicles, some control design strategies have been exploited in the literature. Yuan and Zhu (2016) proposed a lateral-longitudinal control scheme using automatic steering strategies to avoid jackknifing, considering input limitations. Michałek (2014) presented a highly scalable nonlinear cascade-like control to solve the path-following problem for articulated robotic vehicles equipped with arbitrary number of off-axle hitched trailers. With respect to the path-following problem for articulated vehicles, an active steering controller of the tractor and trailer based on LQR was designed by Kim et al. (2016), whilst a novel sliding mode controller was proposed by Nayl, Nikolakopoulos, Gustafsson, Kominiak, and Nyberg (2018). However, the autonomous control of articulated heavy-duty vehicles remains an issue. As payload may be much greater than vehicle weight itself (Kati et al., 2016), mass is a critical parameter in vehicle dynamics and those vehicles are especially affected by mass variations. Hence, a control technique that overcomes the parametric uncertainties in the vehicle model is necessary to ensure system stability and performance objectives for a range of parameter values (Kati et al., 2016). This leads to the need of robust controllers designed to withstand mass variations.

Kati et al. (2016) proposed an $\mathcal{H}_\infty$ controller to deal with uncertainties on payload of the vehicle. However, as the $\mathcal{H}_\infty$ controller depends on the offline adjustment of the auxiliary parameter γ, this results in sub-optimal controller operation due to the mass variations. The $\mathcal{H}_\infty$ controller is furthermore robust, but it cannot ensure smoothness for steering control applications. In fact, the lower the γ value, the more optimality condition the controller reaches. On the other hand, it cannot guarantee driving smoothness as there is no parameter to deal with this. Consequently, a mixed $\mathcal{H}_2/\mathcal{H}_\infty$ controller is used in the literature, where smoothness, and robustness and optimisation are respectively handled (Scherer, 1995). In order to address the sub-optimality problem, the contribution of this paper is a novel approach for the lateral control of an autonomous articulated heavy-duty vehicle, based on a Robust Linear Quadratic Regulator (RLQR) presented in Terra, Cerri, and Ishihara (2014) and Cerri, Terra, and Ishihara (2009). The main advantage of the proposed controller is that it does not require any auxiliary tuning parameters, since both smoothness and robustness are already foreseen through a certain penalty parameter μ, which vanishes in the limit when it tends to infinity. This feature maintains the optimality for the full range of parametric uncertainties. This is additionally useful for online applications. A continuous-time model for the articulated vehicle in state-space form is presented. Then, the model is discretised in order to apply discrete RLQ control for solving a path-following problem.

Since $\mathcal{H}_\infty$ control is widely used for path-tracking problems (Hu et al., 2016) and for robustifying the control strategy in automotive applications (Li, Jing, Wang, & Chen, 2018; Zhao, Zhang, & Li, 2018), a standard $\mathcal{H}_\infty$ controller is also applied to the same plant for the sake of comparison. Uncertainties on vehicle mass are introduced, then the performance of both controllers is compared in different cases. Simulation tests evaluate robustness, steering behaviour, truck displacement error and orientation error.

The RLQR ensures stability for a range of possible payloads. On the other hand, the $\mathcal{H}_\infty$ controller is dependent on the auxiliary parameter γ. Therefore, it cannot maintain good performance (or even stability) for a wide range of payloads, unless γ is adjusted offline (Terra et al., 2014).

The paper is organised as follows: Section 2 presents both the model of a heavy articulated vehicle in continuous-time state-space form and a path-following model, which are properly put together to make a single model; Section 3 exhibits the RLQR, showing how it is derived from a quadratic cost function and a robust regularised least squares problem; Section 4 shows and discusses the application of the RLQR and its results compared to an $\mathcal{H}_\infty$ controller; Section 5 brings the conclusions.

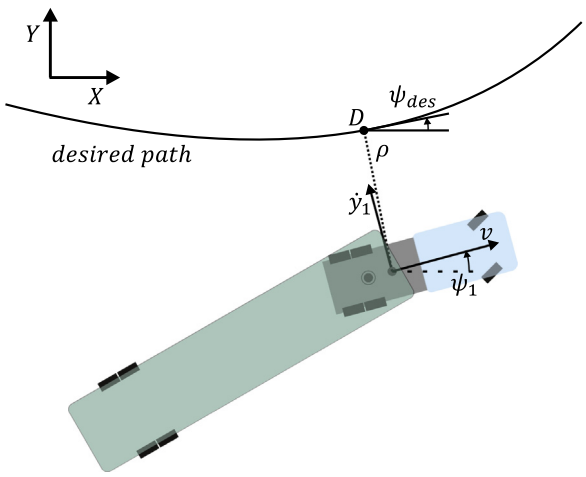

Fig. 1. Schematic diagram for path-following model.

2. System modelling

With the aim to make the articulated heavy-duty vehicle follow a desired path, it is not only necessary to minimise the lateral offset and heading error, but also ensure the vehicle stability. Therefore, the system modelling must take into account the path following and dynamic variables. This section introduces the vehicle model for simulations and control design.

2.1. Path-following model

In order to solve the path-following problem, the lateral controller aims to reduce lateral displacement and orientation angle errors of the towing vehicle. Therefore, the path-following model adopted here is based on the equations presented by Skjetne and Fossen (2001). Fig. 1 shows the schematic diagram of path-following model for an articulated vehicle, where $\dot{y}_1$ is tractor lateral velocity and v is tractor longitudinal velocity. The lateral displacement of the vehicle to a given reference path is the distance ρ from tractor centre of gravity to the closest point D on the desired path. The tractor orientation error is defined as $\theta = \psi_1 - \psi_{des}$, where ψ_1 and ψ_{des} are the current and desired orientation angles of the tractor, respectively.

Based on Serret–Frenet equations (Skjetne & Fossen, 2001), the path-following model of the autonomous ground vehicle is expressed as

$$\begin{aligned} \dot{\rho} &= v \sin\theta + \dot{y}_1 \cos\theta \\ \dot{\theta} &= \dot{\psi}. \end{aligned} \tag{1}$$

The displacement error ρ can be rewritten in the linear form by assuming that the orientation error θ is small, as follows

$$\dot{\rho} = v\theta + \dot{y}_1. \tag{2}$$

2.2. Articulated vehicle model

Single-track models are widely used in literature (Alcala et al., 2018; Ji et al., 2018; Jujnovich & Cebon, 2013; Kati et al., 2016) to describe the vehicle lateral behaviour without much modelling and parametrisation effort (Schramm, Hiller, & Bardini, 2018). These assume that the vehicle can be described by only one equivalent track in each axle, linked by the vehicle body. Consequently, it only takes into account the planar movement of the vehicle, disregarding roll and pitch effects. The nonholonomic linear model adopted here is based on bicycle model presented by van de Molengraft-Luijten, Besselink, Verschuren, and Nijmeijer (2012).

Fig. 2 shows the free body diagram of a vehicle with one articulation, where the following assumptions are adopted:

$$\begin{bmatrix} m_1+m_2 & -m_2(h_1+a_2) & -m_2a_2 & 0 & 0 & 0 \\ -m_2h_1 & J_1+m_2h_1(h_1+a_2) & m_2h_1a_2 & 0 & 0 & 0 \\ -m_2a_2 & J_2+m_2a_2(h_1+a_2) & J_2+m_2a_2^2 & 0 & 0 & 0 \\ 0 & 0 & 0 & 1 & 0 & 0 \\ 0 & 0 & 0 & 0 & 1 & 0 \\ 0 & 0 & 0 & 0 & 0 & 1 \end{bmatrix} \dot{x} =$$

$$\begin{bmatrix} \frac{-c_1-c_2-c_3}{v} & \frac{c_3(h_1+l_2)-a_1c_1+b_1c_2-(m_1+m_2)v^2}{v} & \frac{c_3l_2}{v} & c_3 & 0 & 0 \\ \frac{c_3h_1-a_1c_1+b_1c_2}{v} & \frac{m_2h_1v^2-a_1^2c_1-b_1^2c_2-c_3h_1(h_1+l_2)}{v} & \frac{-c_3h_1l_2}{v} & -c_3h_1 & 0 & 0 \\ \frac{c_3l_2}{v} & \frac{m_2a_2v^2-c_3l_2(h_1+l_2)}{v} & \frac{-c_3l_2^2}{v} & -c_3l_2 & 0 & 0 \\ 0 & 0 & 1 & 0 & 0 & 0 \\ 1 & 0 & 0 & 0 & 0 & v \\ 0 & 1 & 0 & 0 & 0 & 0 \end{bmatrix} x + \begin{bmatrix} c_1 \\ a_1c_1 \\ 0 \\ 0 \\ 0 \\ 0 \end{bmatrix} \alpha, \tag{4}$$

Box I.

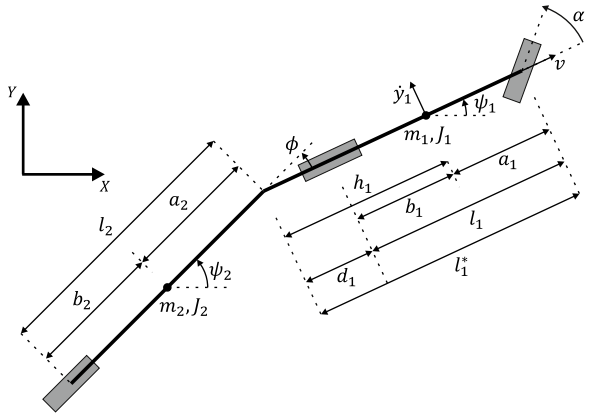

Fig. 2. Articulated vehicle single-track model.

- Differences between left and right tracks are ignored;
- Vehicle velocity parameter is constant;
- The mass of each unit is assumed to be concentrated at the centre of gravity;
- Lateral tyre forces are proportional to the tyre slip angles;
- There is no load transfer.

Table 1 details the parameters of the articulated vehicle shown in Fig. 2. Note that hitch point may be positioned behind the towing vehicle rear axle (e.g. truck-full trailers where $h_1 > b_1$ and $d_1 > 0$) or in front of it (e.g. tractor–semitrailers where $h_1 < b_1$ and $d_1 < 0$).

In order to improve the path following, lateral displacement ρ and orientation error θ must be as small as possible. In addition, it is necessary to ensure vehicle stability. Hence, the lateral velocity $\dot{y}_1$, yaw rate $\dot{\psi}_1$, articulation angle rate $\dot{\phi}$ and articulation angle ϕ must be well controlled.

The motion equation of the articulated vehicle can be expressed as

$$M\dot{x} = Ax + B\alpha, \tag{3}$$

with the state vector defined as $x = [\dot{y}_1, \dot{\psi}_1, \dot{\phi}, \phi, \rho, \theta]^T$. Therefore, the state-space description of the path-following model for the articulated heavy-duty vehicle is written as Eq. (4) given in Box I, where the vehicle steering angle α is the control input, c_1, c_2 and c_3 are the cornering stiffness of the tractor front axle, tractor rear axle and trailer axle, respectively.

Table 1
Description of vehicle parameters.

Parameter	Meaning	Unit
a_1	Distance from the front axle to the tractor centre of gravity	m
a_2	Distance from the coupling point to the trailer centre of gravity	m
b_1	Distance from the tractor rear axle to the tractor centre of gravity	m
b_2	Distance from the trailer axle to the trailer centre of gravity	m
l_1	Tractor wheelbase	m
l_2	Trailer wheelbase	m
d_1	The distance between the tractor rear axle and the coupling point	m
h_1	The distance between coupling point and the tractor centre of gravity	m
l_1^*	The distance between the tractor front axle and the coupling point	m
v	Forward velocity	m/s
$\dot{y}_1$	Lateral velocity	m/s
m_1	Tractor mass	kg
m_2	Trailer mass	kg
J_1	Tractor moment of inertia	kg m^2
J_2	Trailer moment of inertia	kg m^2
ψ_1	Tractor yaw	rad
ψ_2	Trailer yaw	rad
α	Steering angle	rad
ϕ	Articulation angle	rad

Many studies consider constant cornering stiffness. However, this hypothesis is not considered in this work since these coefficients may vary according to several vehicle parameters. In fact, Fancher demonstrated in Fancher (1989) (as cited in Luijten, 2010) that the relation between the tyre cornering stiffness and the vertical load forces is approximately linear for truck tyres. The coefficient of proportionality is given by a normalised cornering stiffness f_j, and the cornering stiffness c_j scales linearly with the vertical load force of the axle F_{z_j}. Therefore, the cornering stiffness parameters are calculated as:

$$c_j = f_j F_{z_j} \text{ with } j = 1, \ldots, p, \tag{5}$$

where p is the number of axles in the vehicle, $j = 1$ corresponds to the tractor front axle, $j = 2$ to the tractor rear axle and $j = 3$ to the trailer axle.

The vertical force in each axle can be calculated as

$$\begin{aligned} F_{z_1} &= m_1 g \frac{b_1}{l_1} - m_2 g \frac{b_2 d_1}{l_2 l_1} \\ F_{z_2} &= m_1 g \frac{a_1}{l_1} + m_2 g \frac{b_2 l_1^*}{l_2 l_1} \\ F_{z_3} &= m_2 g \frac{a_2}{l_2}, \end{aligned} \tag{6}$$

where g is the gravitational acceleration. Moreover, Houben (2008) (as cited in van de Molengraft-Luijten et al., 2012) observed that the normalised cornering stiffness of trailer tyres, drive and steer are approximately the same. Therefore, it is assumed $f_1 \approx f_2 \approx f_3$.

Nevertheless, a discrete state-space representation of the system is necessary in order to perform the robust recursive control for time-varying linear systems subject to parametric uncertainties. Hence, the System (4) is discretised by using the Tustin method.

3. Robust recursive regulator

The goal of the Robust Linear Quadratic Regulator (RLQR) is to minimise a given cost function subject to the maximum influence of parametric uncertainties. It is made by implementing an optimal feedback law in the form $u_i = K_i x_i$, where K_i is the feedback gain. This section describes the robust recursive regulator presented by Terra et al. (2014) and Cerri et al. (2009).

3.1. Problem formulation

Consider the following discrete-time linear system subject to parametric uncertainties

$$x_{i+1} = (F_i + \delta F_i)x_i + (G_i + \delta G_i)u_i, \tag{7}$$

where $i = 0, \dots, N$, $x_i \in \mathbb{R}^n$ is the state vector, $u_i \in \mathbb{R}^m$ is the control input, and $F_i \in \mathbb{R}^{n\times n}$ and $G_i \in \mathbb{R}^{n\times m}$ are known nominal model matrices. Uncertainty matrices δF_i and δG_i represent parametric uncertainties modelled as

$$\begin{bmatrix} \delta F_i & \delta G_i \end{bmatrix} = H_i \Delta_i \begin{bmatrix} E_{F_i} & E_{G_i} \end{bmatrix}, \tag{8}$$

where $i = 0, \dots, N$; $H_i \in \mathbb{R}^{n\times p}$; $E_{F_i} \in \mathbb{R}^{l\times n}$ and $E_{G_i} \in \mathbb{R}^{l\times m}$ are known matrices; and and $\Delta_i \in \mathbb{R}^{p\times l}$ is an arbitrary matrix such that $\|\Delta\| \leq 1$.

In order to obtain the Robust Linear Quadratic Regulator, the following optimisation problem must be solved (Terra et al., 2014):

$$\min_{x_{i+1}, u_i} \max_{\delta F_i, \delta G_i} \bar{J}_i^{\mu}(x_{i+1}, u_i, \delta F_i, \delta G_i), \tag{9}$$

where $\bar{J}_i^{\mu}$ is the cost function

$$\begin{aligned} &\bar{J}_i^{\mu}(x_{i+1}, u_i, \delta F_i, \delta G_i) = \\ &\begin{bmatrix} x_{i+1} \\ u_i \end{bmatrix}^T \begin{bmatrix} P_{i+1}^r & 0 \\ 0 & R_i \end{bmatrix} \begin{bmatrix} x_{i+1} \\ u_i \end{bmatrix} + \boldsymbol{\Phi}^T \begin{bmatrix} Q_i & 0 \\ 0 & \mu I \end{bmatrix} \boldsymbol{\Phi}, \end{aligned} \tag{10}$$

with fixed penalty parameter $\mu > 0$, weighing matrices $Q_i \succ 0$, $R_i \succ 0$, $P_{i+1} \succ 0$ and

$$\boldsymbol{\Phi} = \left\{ \begin{bmatrix} 0 & 0 \\ I & -G_i - \delta G_i \end{bmatrix} \begin{bmatrix} x_{i+1} \\ u_i \end{bmatrix} - \begin{bmatrix} -I \\ F_i + \delta F_i \end{bmatrix} x_i \right\}.$$

Details on penalty function can be seen in Cerri et al. (2009).

Remark. The optimisation problem (9)–(10) is a particular case of the robust least-squares problem and will be treated below.

3.2. Regularised least squares

Consider the least squares minimisation problem defined by

$$\min_{x\in\mathbb{R}^m} \{J(x)\}, \tag{11}$$

where $J(x)$ is a regularised quadratic functional

$$\begin{aligned} J(x) &= \|x\|_Q^2 + \|Ax - b\|_W^2 \\ &= x^T Q x + (Ax - b)^T W (Ax - b), \end{aligned} \tag{12}$$

with $Q \in \mathbb{R}^{m\times m}$ (regularisation matrix) and $W \in \mathbb{R}^{m\times n}$ symmetric positive definite, $A \in \mathbb{R}^{n\times n}$ and $b \in \mathbb{R}^n$ known, and $x \in \mathbb{R}^m$ the unknown vector.

Lemma 3.1. *The optimal solution for the problem (11)–(12) is*

$$x^* = \left(Q + A^T W A\right)^{-1} A^T W b.$$

Proof. See Kailath, Sayed, and Hassibi (2000). □

3.3. Robust regularised least-squares problem

In the regularised least-squares problem established in (11)–(12), now suppose that the matrix A and the vector b are under influence of uncertainties δA and δb, respectively. Consider the min–max optimisation problem defined in Sayed and Nascimento (1999) in the form:

$$\min_x \max_{\delta A, \delta b} \{J(x, \delta A, \delta b)\}, \tag{13}$$

with $J(x, \delta A, \delta b)$ given by

$$J(x, \delta A, \delta b) = \|x\|_Q^2 + \|(A + \delta A)x - (b + \delta b)\|_W^2, \tag{14}$$

and the uncertainties δA and δb modelled as

$$\begin{bmatrix} \delta A & \delta b \end{bmatrix} = H \Delta \begin{bmatrix} E_A & E_b \end{bmatrix}, \tag{15}$$

with A, b, H, E_A, E_b, Q and W known matrices, Δ an arbitrary contraction matrix ($\|\Delta\| \leq 1$) and x an unknown vector. The optimal solution for the problem (13)–(15) is given below. See demonstration details in Sayed and Nascimento (1999), where a general result is proposed.

Lemma 3.2. *The optimisation problem (13)–(15) has a unique solution*

$$x^* = \left(\hat{Q} + A^T \hat{W} A\right)^{-1} \left(A^T \hat{W} b + \hat{\lambda} E_A^T E_b\right),$$

with $\hat{Q}$ and $\hat{W}$ defined as

$$\begin{aligned} \hat{Q} &:= Q + \hat{\lambda} E_A^T E_A, \\ \hat{W} &:= W + W H (\hat{\lambda} I - H^T W H)^{\dagger} H^T W. \end{aligned}$$

The non-negative scalar parameter obtained from the minimisation problem

$$\hat{\lambda} = \arg \min_{\lambda \geq \|H^T W H\|} \{\Gamma(\lambda)\},$$

where $\Gamma(\lambda) := \|x(\lambda)\|_Q^2 + \lambda \|E_A x(\lambda) - E_b\|^2 + \|Ax(\lambda) - b\|_{W(\lambda)}^2$ with

$$\begin{aligned} Q(\lambda) &:= Q + \lambda E_A^T E_A, \\ \tilde{Q}(\lambda) &:= Q(\lambda) + A^T W(\lambda) A, \\ W(\lambda) &:= W + W H (\lambda I - H^T W H)^{\dagger} H^T W, \\ x(\lambda) &:= \tilde{Q}(\lambda)^{-1} \left(A^T W(\lambda) b + \lambda E_A^T E_b\right). \end{aligned}$$

Proof. See Sayed and Nascimento (1999) □

For this type of problem, it is appropriate to redefine Lemma 3.2 in terms of an array of matrices. The following lemma shows an optimal solution for the problem (13)–(15) in an alternative structure to this fundamental theorem.

Lemma 3.3. *Suppose $Q \succ 0$ and $W \succ 0$. The solution x^* for the problem (13)–(15) can be rewritten as*

$$\begin{bmatrix} x^* \\ J(x^*) \end{bmatrix} = \begin{bmatrix} 0 & 0 \\ 0 & b \\ 0 & E_b \\ I & 0 \end{bmatrix}^T \begin{bmatrix} Q^{-1} & 0 & 0 & I \\ 0 & \hat{W}^{-1} & 0 & A \\ 0 & 0 & \hat{\lambda}^{-1} I & E_A \\ I & A^T & E_A^T & 0 \end{bmatrix}^{-1} \begin{bmatrix} 0 \\ b \\ E_b \\ 0 \end{bmatrix},$$

with $\hat{W}$ and $\hat{\lambda}$ as in Lemma 3.2.

Proof. See Cerri et al. (2009). □

3.4. Robust linear quadratic regulator

The optimisation problem (9)–(10) is solved based on the solution of a general robust regularised least-squares problem (Terra et al., 2014). Back to the solution presented in Lemma 3.2, with $\mu > 0$, the RLQR has an optimal operation point for each step k of the algorithm. When suitable identifications of (9)–(10) with (13)–(15) are carried out, the regularisation of the robust regulator is reached thanks to minimisation over both $x_{i+1}(\mu)$ and $u_i(\mu)$ (Terra et al., 2014):

$$Q \leftarrow \begin{bmatrix} P_{i+1} & 0 \\ 0 & R_i \end{bmatrix}, \; x \leftarrow \begin{bmatrix} x_{i+1}(\mu) \\ u_k(\mu) \end{bmatrix}, W \leftarrow \begin{bmatrix} Q_i & 0 \\ 0 & \mu I \end{bmatrix},$$

$$A \leftarrow \begin{bmatrix} 0 & 0 \\ I & -G_i \end{bmatrix}, \; \delta A \leftarrow \begin{bmatrix} 0 & 0 \\ 0 & -\delta G_i \end{bmatrix}, \; \Delta \leftarrow \Delta_i,$$

$$b \leftarrow \begin{bmatrix} -I \\ F_i \end{bmatrix} x_i, \; \delta b \leftarrow \begin{bmatrix} 0 \\ \delta F_i \end{bmatrix} x_i,$$

$$H \leftarrow \begin{bmatrix} 0 \\ H_i \end{bmatrix}, \; E_A \leftarrow \begin{bmatrix} 0 & -E_{G_i} \end{bmatrix}, \; E_b \leftarrow E_{F_i} x_i, \tag{16}$$

The following theorem shows a framework given in terms of an array of matrices with the purpose of calculating the optimal cost function, control input and state trajectory.

Theorem 3.1. *For each $\mu > 0$ in the optimisation problem (9)–(10), the optimal solution is given by*

$$\begin{bmatrix} x^*_{i+1}(\mu) \\ u^*_i(\mu) \\ \tilde{J}^{\mu}_i(x^*_{i+1}(\mu), u^*_i(\mu)) \end{bmatrix} = \begin{bmatrix} I & 0 & 0 \\ 0 & I & 0 \\ 0 & 0 & x_i(\mu)^T \end{bmatrix}^T \begin{bmatrix} L_{i,\mu} \\ K_{i,\mu} \\ P_{i,\mu} \end{bmatrix} x_i, \tag{17}$$

where the closed-loop system matrix L_i and the feedback gain K_i result from the recursion

$$\begin{bmatrix} L_i \\ K_i \\ P_i \end{bmatrix} = \begin{bmatrix} 0 & 0 & -I & \mathcal{F}_i & 0 & 0 \\ 0 & 0 & 0 & 0 & 0 & I \\ 0 & 0 & 0 & 0 & I & 0 \end{bmatrix} \Xi^{-1} \begin{bmatrix} 0 \\ 0 \\ -I \\ \mathcal{F}_i \\ 0 \\ 0 \end{bmatrix}, \tag{18}$$

with

$$\Xi = \begin{bmatrix} P^{-1}_{i+1} & 0 & 0 & 0 & I & 0 \\ 0 & R^{-1}_i & 0 & 0 & 0 & I \\ 0 & 0 & Q^{-1}_i & 0 & 0 & 0 \\ 0 & 0 & 0 & \Sigma_i(\mu, \hat{\lambda}_i) & \mathcal{I} & -\mathcal{G}_i \\ I & 0 & 0 & \mathcal{I}^T & 0 & 0 \\ 0 & I & 0 & -\mathcal{G}^T & 0 & 0 \end{bmatrix},$$

$$\Sigma_i = \begin{bmatrix} \mu^{-1} I - \hat{\lambda}^{-1}_i H_i H_i^T & 0 \\ 0 & \hat{\lambda}^{-1}_i I \end{bmatrix},$$

$$\mathcal{I} = \begin{bmatrix} I \\ 0 \end{bmatrix}, \; \mathcal{G}_i = \begin{bmatrix} G_i \\ E_{G_i} \end{bmatrix}, \; \mathcal{F}_i = \begin{bmatrix} F_i \\ E_{F_i} \end{bmatrix},$$

where P_{i+1} is the solution of the associated Riccati Equation and $\lambda_i > \|\mu H_i^T H_i\|$ (Sayed, 2001). Furthermore, alternatively one has

$$\begin{aligned} P_{i,\mu} =& L^T_{i,\mu} P_{i+1} L_{i,\mu} + K_{i,\mu} R_i K_{i,\mu} + Q_i + \\ & (\mathcal{I} L_{i,\mu} - \mathcal{G}_i K_{i,\mu} - \mathcal{F}_i)^T \Sigma^{-1}_{i,\mu} (\mathcal{I} L_{i,\mu} - \mathcal{G}_i K_{i,\mu} - \mathcal{F}_i) \succ 0. \end{aligned} \tag{19}$$

Proof. It follows from Lemma 3.3, identifications performed in (16) and results shown in Cerri et al. (2009). □

Algorithm 1 shows the Robust Linear Quadratic Regulator obtained with Lemma 3.2. The parameter μ is associated with system robustness. It is responsible for ensuring the RLQR regularisation and validity of the equality (7). For maximum robustness, $\mu \to \infty$ and consequently $\Sigma_i \to 0$.

For each iteration of (19), the matrix $P_{i,\mu}$ is finite and $\mathcal{I} L_{i,\mu} - \mathcal{G}_i K_{i,\mu} - \mathcal{F}_i \to 0$, as shown in Terra et al. (2014). Therefore,

$$\begin{aligned} & L_{i,\infty} = F_i + G_i K_{i,\infty} \\ & E_{F_i} + E_{G_i} K_{i,\infty} = 0, \end{aligned} \tag{20}$$

and a sufficient condition that satisfy (20) is

$$rank\left(\begin{bmatrix} E_{F_i} & E_{G_i} \end{bmatrix}\right) = rank\left(E_{G_i}\right). \tag{21}$$

Convergence and stability analyses of the RLQR are made through direct comparison with the standard optimal regulator problem for systems not subject to uncertainties. It resembles the standard LQR where the stability is directly related with the positiveness of the Riccati equation solution (Terra et al., 2014). More details on convergence and stability analysis can be found in Terra et al. (2014).

4. Numerical results and discussion

For the controller validation, the RLQR was performed and compared with the $\mathcal{H}_\infty$ controller in various operational conditions. The Matlab/Simulink simulation software was used for this purpose. Simulations consist of minimising the lateral displacement and orientation errors. A double lane-change manoeuvre was performed during 30 s with the sampling period being 0.01 s and the nominal payload subject to uncertainties. Fig. 3 shows the scenario of studied cases, where ε is the tractor width. Furthermore, Table 2 shows the vehicle parameters and the necessary information to calculate them, obtained from websites for commercial vehicles[1] and towing implement[2] manufacturers. For all cases, the initial conditions are the same for both controllers, those being $x_0 = [0, 0, 0, 0, 0.3, -0.1]^T$, the penalty parameter $\mu = 10^8$,

$$H = \begin{bmatrix} 1 \\ 1 \\ 1 \\ 1 \\ 1 \\ 1 \end{bmatrix}, \; E_F = \begin{bmatrix} 6.8572 \times 10^{-5} \\ -8.6201 \times 10^{-5} \\ -2.1440 \times 10^{-5} \\ -10.4924 \times 10^{-5} \\ 0 \\ -666.66667 \times 10^{-5} \end{bmatrix}^T \text{ and } E_G = \begin{bmatrix} -666.66667 \times 10^{-5} \\ -666.66667 \times 10^{-5} \end{bmatrix}^T.$$

The methodology used to calculate the uncertainty matrices is described in Appendix A.

The uncertainty parameters were chosen as vectors, this implies that the condition of existence of the controller (21) is satisfied, regardless of the numerical values of the uncertainty parameters.

The normalised cornering stiffness was applied in all cases studied here as it is a satisfactory representation for most applications and conditions (Luijten, 2010). Thus, it was calculated as a function of vertical load by assuming $f = f_1 = f_2 = f_3 = 5.73\ \text{rad}^{-1}$. In addition, the maximum steering angle (0.44 rad) was taken into account in numerical results.

The linear system must be rewritten in order to compare the $\mathcal{H}_\infty$ control and the robust recursive regulator presented in this paper. Thus, the robust control design considering the $\mathcal{H}_\infty$ method discussed by Hassibi, Sayed, and Kailath (1999) was used. Its equations and formulation are given in Appendix B.

Fig. 4 gives the block diagrams for both control techniques, where e_i is the error between the reference and output, and x_{ref} is the reference state vector. Since we aim to minimise the state variable errors, the control law is $u_i = K_i e_i$. Both e_i and x_{ref} are obtained when a reference control signal is applied to the lateral model of the vehicle.

[1] https://www.scania.com.
[2] http://www.librelato.com.br.

Algorithm 1: The Robust Linear Quadratic Regulator

Uncertain model: Consider the model (7)–(8) and criterion (9)–(10) with known F_i, G_i, E_{F_i}, E_{G_i}, $Q_i \succ 0$, and $R_i \succ 0$ for all i.

Initial conditions: Define x_0 and $P_{i,N} \succeq 0$.

Step 1: *(Backward)* For all $i = N-1, \ldots, 0$, compute

$$\begin{bmatrix} L_i \\ K_i \\ P_i \end{bmatrix} = \begin{bmatrix} 0 & 0 & 0 \\ 0 & 0 & 0 \\ 0 & 0 & -I \\ 0 & 0 & F_i \\ 0 & 0 & E_{F_i} \\ I & 0 & 0 \\ 0 & I & 0 \end{bmatrix}^T \begin{bmatrix} P_{i+1}^{-1} & 0 & 0 & 0 & 0 & I & 0 \\ 0 & R_i^{-1} & 0 & 0 & 0 & 0 & I \\ 0 & 0 & Q_i^{-1} & 0 & 0 & 0 & 0 \\ 0 & 0 & 0 & 0 & 0 & I & -G_i \\ 0 & 0 & 0 & 0 & 0 & 0 & -E_{G_i} \\ I & 0 & 0 & I & 0 & 0 & 0 \\ 0 & I & 0 & -G_i^T & -E_{G_i}^T & 0 & 0 \end{bmatrix}^{-1} \begin{bmatrix} 0 \\ 0 \\ -I \\ F_i \\ E_{F_i} \\ 0 \\ 0 \end{bmatrix}.$$

Step 2: *(Forward)* For each $i = 0, \ldots, N-1$, obtain

$$\begin{bmatrix} x_{i+1}^* \\ u_i^* \end{bmatrix} = \begin{bmatrix} L_i \\ K_i \end{bmatrix} x_i^*,$$

with the total cost given by $J_r^* = x_0^T P_0 x_0$.

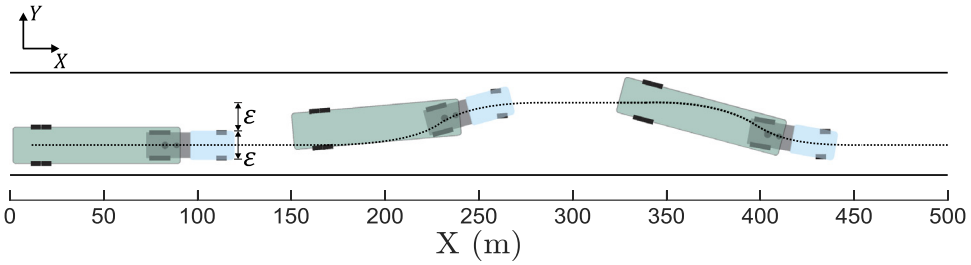

Fig. 3. Double lane change scenario.

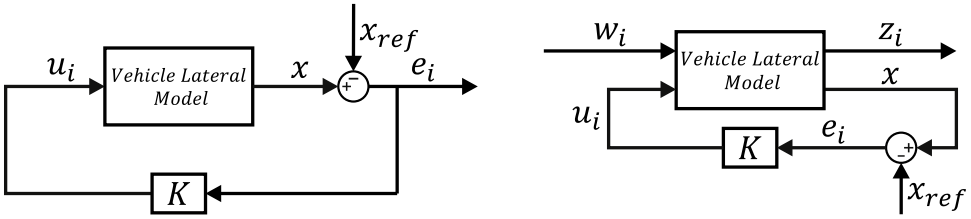

(a) RLQR block diagram. (b) $\mathcal{H}_\infty$ control system block diagram.

Fig. 4. Block diagrams for Robust Linear Quadratic Regulator and $\mathcal{H}_\infty$ control systems.

Table 2
Vehicle parameters values.

Parameter	Value
a_1	1.734 m
a_2	4.8 m
b_1	2.415 m
b_2	3.2 m
l_1	4.149 m
l_2	8.0 m
d_1	−0.29 m
h_1	2.125 m
l_1^*	3.859 m
ϵ	2.6 m
v	16.667 m/s
m_1	8909 kg
m_2	9370 kg
Payload	24 000 kg
J_1	41 566 kg m^2
J_2	404 360 kg m^2
c_1	345 155 N/rad
c_2	927 126 N/rad
c_3	1 158 008 N/rad

4.1. System response

The articulated heavy vehicle behaviour was evaluated with numerical results by taking a given reference path. For this purpose, the lateral velocity, yaw rate, articulation angle rate, articulation angle, lateral displacement and orientation error of the vehicle were observed. Moreover, controller evaluation was done through graphic analysis, and by adopting maximum steering rate and $\mathcal{L}_2$ norm of the error as performance criteria.

Tables 3 and 4 show maximum steering rate, payload variations, and $\mathcal{L}_2$ norm of lateral displacement and orientation errors for both performed controllers, respectively. Payload values for every evaluated case were chosen for the best illustration of the influence of mass variation.

The nominal payload was applied, and the weight matrices Q and R were adjusted so that the maximum steering rate was $max\|\dot{u}\|_{RLQR} \approx 0.3432$ rad/s. In addition, the direct counterpart weight matrices R^c and Q^c have the same values adjusted in Q and R, respectively. Moreover, the robustness parameter γ was adjusted to the lowest possible value

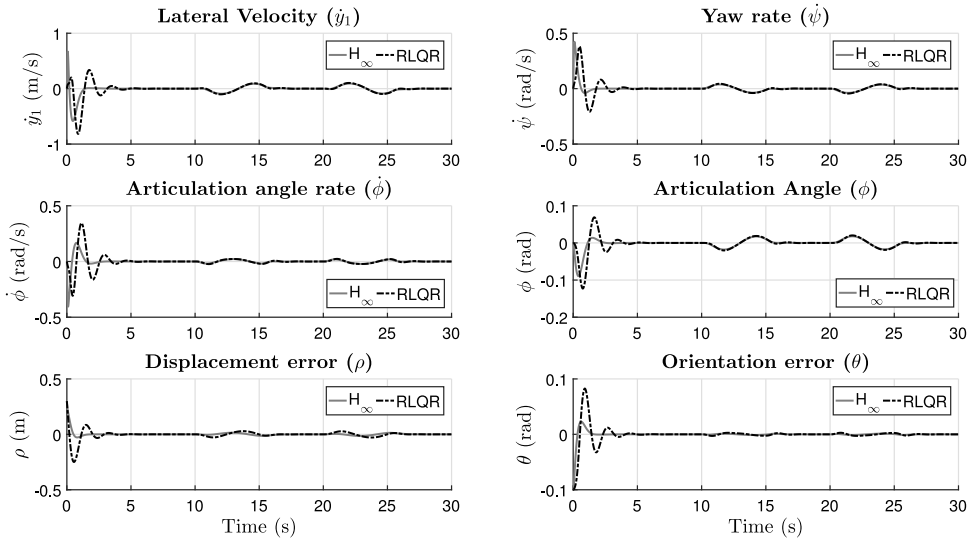

Fig. 5. System state variables for case 1.

Table 3
Evaluated cases for both controllers.

Case	Payload	$max\|\dot{\alpha}_{RLQR}\|$	$max\|\dot{\alpha}_{\mathcal{H}_\infty}\|$
1	100%	0.3432 rad/s	4.3750 rad/s
2	234%	0.4130 rad/s	8.4404 rad/s
3	237%	0.4164 rad/s	9.2350 rad/s
4	0%	0.3333 rad/s	4.5959 rad/s

Table 4
$\mathcal{L}_2$ norm of the lateral displacement and orientation errors.

Case	$\|\rho\|_{\mathcal{L}_2}$		$\|\theta\|_{\mathcal{L}_2}$	
	RLQR	$\mathcal{H}_\infty$	RLQR	$\mathcal{H}_\infty$
1	0.3727	0.2004	0.1481	0.0692
2	0.3886	0.1651	0.1331	0.0793
3	0.3882	0.4055	0.1328	0.2594
4	0.3217	0.2348	0.1358	0.0778

that ensures $\mathcal{H}_\infty$ controller existence. Hence, for every case:

$$\gamma = 14350, \quad Q = R^c = \begin{bmatrix} 1 & 0 & 0 & 0 & 0 & 0 \\ 0 & 1 & 0 & 0 & 0 & 0 \\ 0 & 0 & 1 & 0 & 0 & 0 \\ 0 & 0 & 0 & 1 & 0 & 0 \\ 0 & 0 & 0 & 0 & 25000 & 0 \\ 0 & 0 & 0 & 0 & 0 & 100 \end{bmatrix} \text{ and}$$

$$R = Q^c = \begin{bmatrix} 67070 & 0 \\ 0 & 67070 \end{bmatrix}.$$

Graphics of numerical results for each evaluated case and their case descriptions follow.

Case 1 Considering nominal payload, Figs. 5 and 6 show the system state variables, the global position of tractor centre of mass and steering angle performed by both controllers.

Case 2 Considering 234% of overload over the payload nominal value, Figs. 7 and 8 show the system state variables, the global position of tractor centre of mass and steering angle performed by both controllers.

Case 3 Considering 237% of overload over the payload nominal value, Figs. 9 and 10 show the system state variables, the global position of tractor centre of mass and steering angle performed by both controllers.

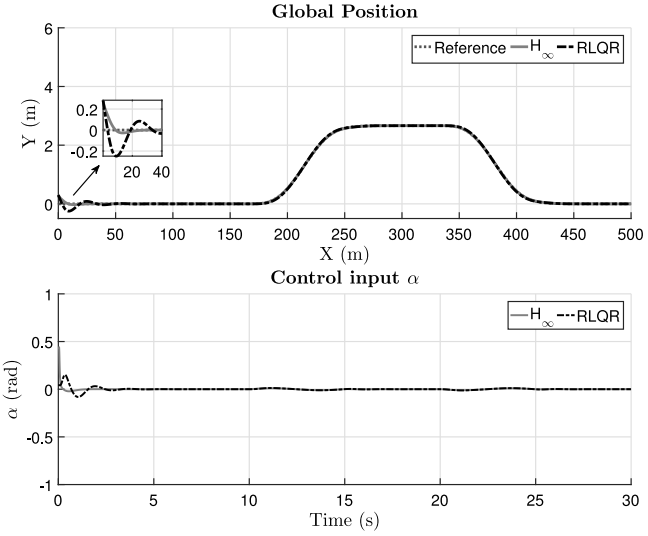

Fig. 6. Global position of the tractor centre of mass and steering angle for case 1.

Case 4 Lastly, considering a vehicle without payload, Figs. 11 and 12 show the system state variables, the global position of the tractor centre of mass and steering angle performed by both controller.

4.2. Discussion

The main goal of these evaluated cases was to show how the Robust Recursive Regulator deals with uncertainties in articulated heavy vehicles. Results demonstrate that the RLQR performance is less affected by payload mass variation than $\mathcal{H}_\infty$ controller. It is verified in Table 4, where the $\mathcal{L}_2$ norm of the lateral displacement and orientation errors of the robust recursive regulator are less affected by mass uncertainties than $\mathcal{H}_\infty$ controller.

Moreover, Table 3 shows that, in the presence of uncertainties, the $max\|\dot{u}_{\mathcal{H}_\infty}\|$ is severely influenced by parametric variations while $max\|\dot{u}_{RLQR}\|$ is much less affected. This is significant, since high steering angle rates mean abrupt driving, which may not be possible for the mechanical system of the vehicle, representing a safety limitation to the $\mathcal{H}_\infty$ controller.

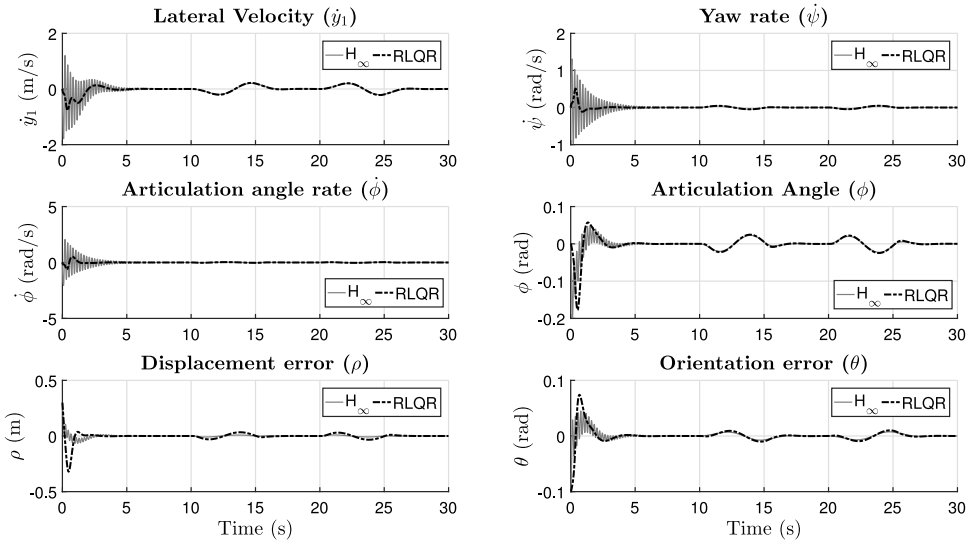

Fig. 7. System state variables for case 2.

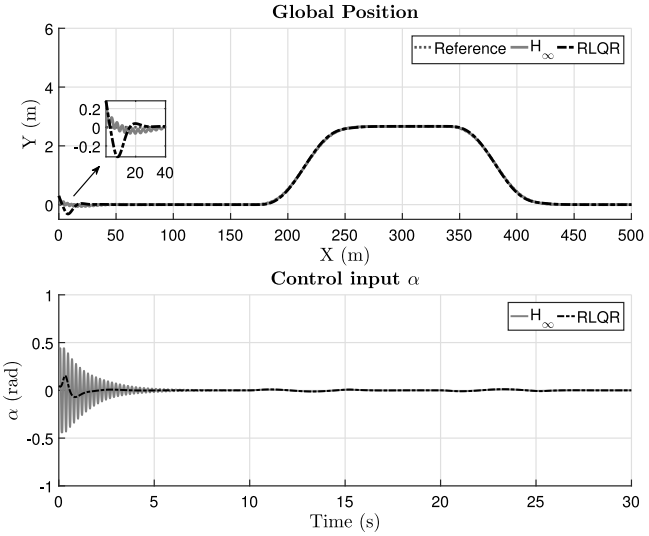

Fig. 8. Global position of the tractor centre of mass and steering angle for case 2.

As shown in Figs. 5, 7, 9 and 11, the performed results for tractor lateral velocity $\dot{y}_1$, tractor yaw rate $\dot{\psi}$, articulation angle rate $\dot{\phi}$ and articulation angle ϕ demonstrate that the robust recursive regulator deals better with vehicle lateral dynamic behaviour since its performance is much less affected by mass variations. Furthermore, the results obtained in Tables 3 and 4 are shown in Figs. 5–12, confirming that the RLQR is still more robust, more stable, smoother and safer than $\mathcal{H}_\infty$ in the presence of payload variations. For better performance of the $\mathcal{H}_\infty$ controller, the parameter γ needs to be adjusted offline for each particular payload. This is very inefficient for practical applications given the wide mass variation in heavy-duty vehicles. The advantage of the RLQR is that it does not require offline adjustment of auxiliary parameters since the penalty parameter μ ensures smoothness and robustness, maintaining the optimality and good performance for each evaluated case.

5. Conclusions

The Robust Linear Quadratic Regulator has been applied to perform the lateral control of an autonomous articulated heavy-duty vehicle subject to parametric uncertainties. Considering uncertainty in the towed

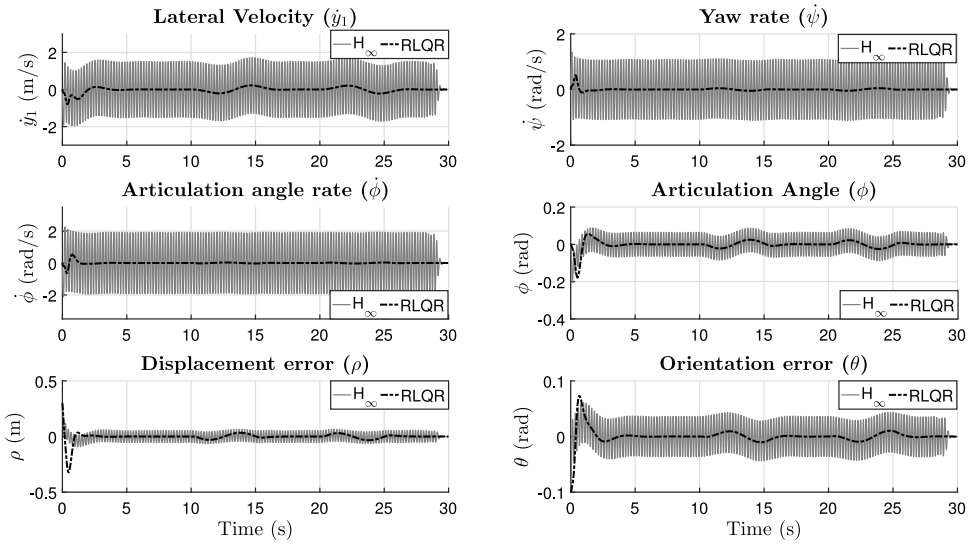

Fig. 9. System state variables for case 3.

$$E_{F_i} = \begin{bmatrix} 1 \\ 1 \\ 1 \\ 1 \\ 1 \\ 0.1 \end{bmatrix}^T \begin{bmatrix} arg\,(|\Gamma_{F_{5,1}}|) & 0 & 0 & 0 & 0 & 0 \\ 0 & arg\,(|\Gamma_{F_{5,2}}|) & 0 & 0 & 0 & 0 \\ 0 & 0 & arg\,(|\Gamma_{F_{5,3}}|) & 0 & 0 & 0 \\ 0 & 0 & 0 & arg\,(|\Gamma_{F_{5,4}}|) & 0 & 0 \\ 0 & 0 & 0 & 0 & arg\,(|\Gamma_{F_{5,5}}|) & 0 \\ 0 & 0 & 0 & 0 & 0 & arg\,(|\Gamma_{F_{5,6}}|) \end{bmatrix} \tag{A.2}$$

Box II.

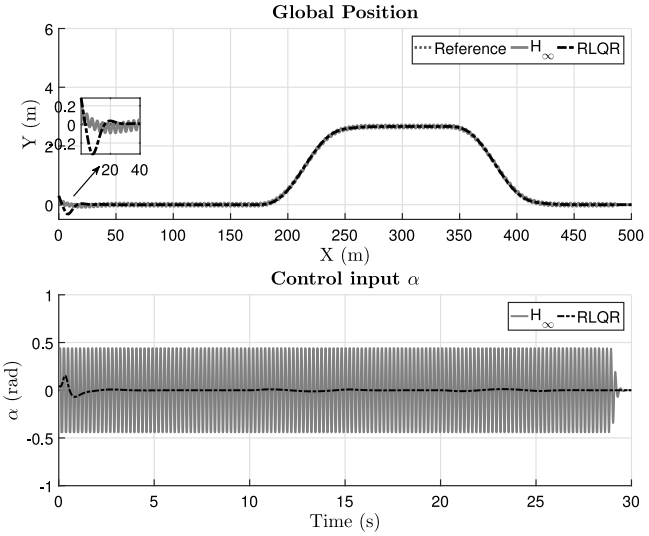

Fig. 10. Global position of the tractor centre of mass and steering angle for case 3.

mass, RLQR controller performance was better in terms of robustness, lateral stability, driving smoothness and safety when compared to the $\mathcal{H}_\infty$ robust control technique. Thus, the robust recursive regulator was demonstrated as a profitable control technique to deal with parametric uncertainties in such vehicle systems. The RLQ controller performs well for a wide range of payloads, while the performance of the H_∞ controller is significantly affected by higher payloads, given a constant γ. Nevertheless, vertical and roll stability cannot be guaranteed because a model-based control design that only considers planar motion was used.

The robust recursive regulator could be exploited in non-articulated and multi-articulated vehicles in order to perform the path-following and lateral control. For future work, the articulated vehicle system will be extended to three-dimensions representation and experimental results will be obtained.

Acknowledgements

This study was financed in part by the Coordenação de Aperfeiçoamento de Pessoal de Nível Superior - Brasil - CAPES (Finance Code 001 and 88887.136349/2017-00), by the São Paulo Research Foundation - FAPESP, Brazil (Grant #2014/50851-0), and by Vale S.A, Brazil.

Conflict of interest

None declared.

Appendix A. Uncertainties matrices

In order to estimate the uncertainties matrices E_F, E_G and H in (8), we considered the inertia uncertainties for deriving a robust control strategy by adopting maximum and minimum values of payload, which results in $m_{p_{max}}$ and $m_{p_{min}}$, respectively. Setting these values of mass, the maximum variations of the matrices F and G are calculated as:

$$\Gamma_F = F_{m_{p_{min}}} - F_{m_{p_{max}}} \tag{A.1}$$

where $F_{m_{p_{min}}}$ and $F_{m_{p_{max}}}$ are the discretised state-space matrices when $m_{p_{max}}$ and $m_{p_{min}}$ are applied to the state-space system (4). Thus, we afterwards selected the row in Γ_F that is most affected by mass variations, here the fifth row.

In this work, $m_{p_{min}}$ and $m_{p_{min}}$ values correspond to the unloaded and 100% of overload vehicle operation. Consequently, this range of uncertainty may imply in large E_F and E_G values, denoted as $E_{F_{100\%}}$ and $E_{G_{100\%}}$. The selection of these values during the control design guarantees the robustness stability for any condition, satisfying the mass variability. However, it jeopardises the performance of the nominal case. Therefore, lower E_F and E_G values were considered to overcome this problem. This choice is capable of enhancing the robustness of the proposal without jeopardising the system performance.

Thus, the matrix E_{F_i} is obtained through Eq. (A.2) in Box II, and E_{G_i} is obtained as:

$$E_{G_i} = \begin{bmatrix} 0.1 \\ 0.1 \end{bmatrix}^T \begin{bmatrix} arg\,\{max(|\Gamma_{F_{5,j}}|)\} & 0 \\ 0 & arg\,\{max(|\Gamma_{F_{5,j}}|)\} \end{bmatrix} \tag{A.3}$$

and $H_i = [1, 1, 1, 1, 1, 1]^T$. This way, the uncertainties matrices are obtained through Eq. (8)

$$\begin{bmatrix} \delta F_i & \delta G_i \end{bmatrix} = H_i \Delta_i \begin{bmatrix} E_{F_i} & E_{G_i} \end{bmatrix},$$

where Δ_i is a scalar represented by the mass variation.

Appendix B. $\mathcal{H}_\infty$ control

The robust control design considering $\mathcal{H}_\infty$ method mentioned in Hassibi et al. (1999) is used for the following linear system

$$x_{i+1} = F_i x_i + G_{1,i} w_i + G_{2,i} u_i, \quad i = 0, \ldots, N, \tag{B.1}$$

where x_i is the state vector, u_i is the control input and w_i is the disturbance. In its sub-optimal formulation, this technique is based on finding a control strategy where for every x_0 and $\{w_i\}_{i=0}^N$,

$$\frac{x_{N+1}^{*T} P_{N+1}^c x_{N+1}^* + \sum_{i=0}^N (u_i^{*T} Q_i^c u_i^* + x_i^{*T} R_i^c x_i^*)}{x_0^{*T} \prod_0^{-1} x_0^* + \sum_{i=0}^N (w_i^{*T} Q_i^w w_i^*)} < \gamma^2, \tag{B.2}$$

for a suitable $\gamma > 0$, where P_{N+1}^c, Q_i^c, R_i^c, Π_0 and Q_i^w are non-negative definite weighing matrices. Such matrices are associated with the final state, control input, state, initial state and disturbance, respectively. The

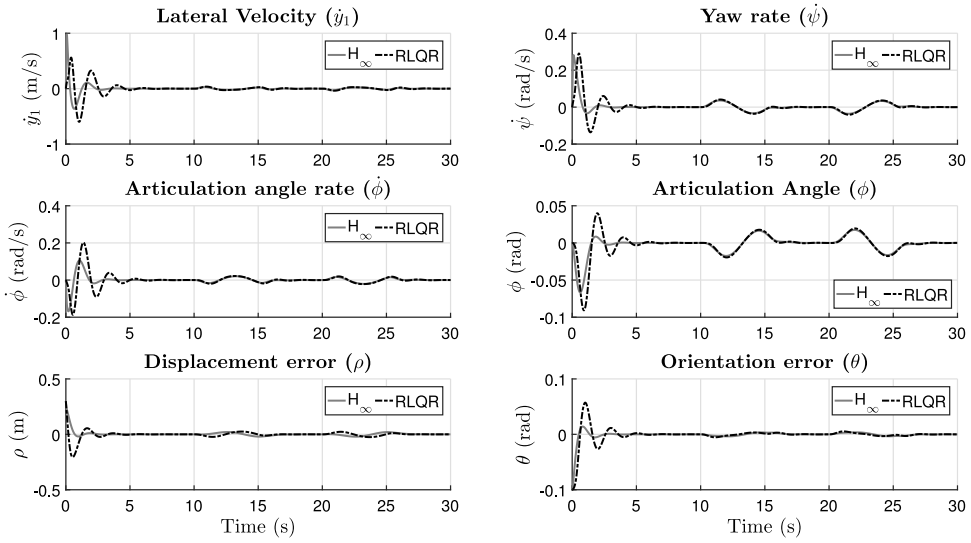

Fig. 11. System state variables for case 4.

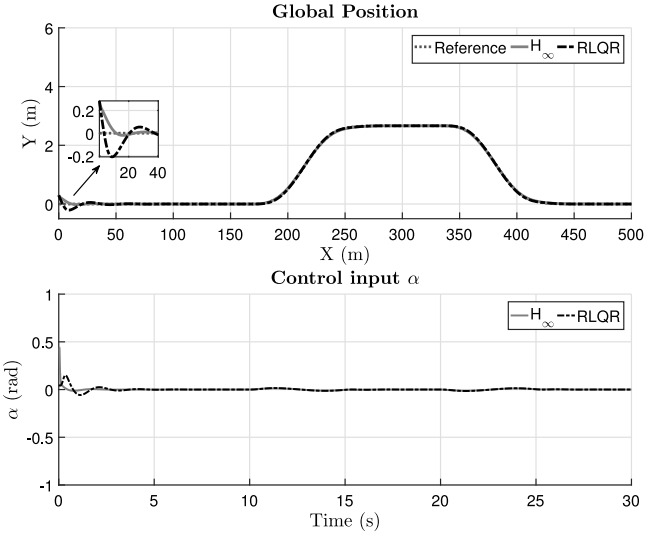

Fig. 12. Global position of the tractor centre of mass and steering angle for case 4.

recursive solution of this problem is formulated in terms of backwards Riccati equation and the verification of some existence conditions is necessary.

To perform the control using this technique, uncertain system (7)–(8) must be rewritten as the system (B.1). Hence, the following immediate are considered

$$\begin{aligned} &F_i \leftarrow F_i, \quad G_{2,i} \leftarrow G_i \quad x_i \leftarrow x_i, \quad u_i \leftarrow u_i, \quad G_{1,i} \leftarrow H_i, \\ &\quad w_i \leftarrow \Delta_i \begin{bmatrix} E_{F_i} & E_{G_i} \end{bmatrix} \begin{bmatrix} x_i \\ u_i \end{bmatrix}, \\ &\quad P^c_{N+1} \leftarrow P_{N+1}, \quad Q^c_i \leftarrow R_i, \quad R^c_i \leftarrow Q_i, \quad Q^w_i \leftarrow I, \quad \Pi_0 \leftarrow I. \end{aligned} \tag{B.3}$$

In order to use the system (B.1) as the uncertain system (7)–(8), some algebraic manipulations are necessary. Considering ${R^c_{G,i}}^{-1} = Q^c_i + G^T_{2,i} P^c_{N+1} G_{2,i}$, the control signal is obtained from Hassibi et al. (1999) as

$$\begin{aligned} u_i &= -{R^c_{G,i}}^{-1} G^T_{2,i} P^c_{N+1} F_i x_i - {R^c_{G,i}}^{-1} G^T_{2,i} P^c_{N+1} G_{1,i} w_i \\ &= (-{R^c_{G,i}}^{-1} G^T_{2,i} P^c_{N+1})(F_i x_i + G_{1,i} w_i). \end{aligned} \tag{B.4}$$

From made in (B.3) substitutions can be made in $G_{1,i}$ and w_i

$$\begin{aligned} u_i &= (-{R^c_{G,i}}^{-1} G^T_{2,i} P^c_{N+1})((F_i + H_i \Delta E_{F_i}) x_i + H_i \Delta E_{G_i} u_{i-1}) \\ &= -{R^c_{G,i}}^{-1} G^T_{2,i} P^c_{N+1} (F_i + \delta F_i) x_i - {R^c_{G,i}}^{-1} G^T_{2,i} P^c_{N+1} H_i \Delta E_{G_i} u_{i-1}, \end{aligned}$$

and adding G_2 in both sides of the equation the (B.4) becomes

$$\begin{aligned} u_i &= -{R^c_{G,i}}^{-1} G^T_{2,i} P^c_{N+1} (F_i + \delta F_i) x_i - {R^c_{G,i}}^{-1} G^T_{2,i} P^c_{N+1} (G_{2,i} + H_i \Delta E_{G_i}) \\ &\quad \times u_{i-1} + {R^c_{G,i}}^{-1} G^T_{2,i} P^c_{N+1} G_{2,i} u_{i-1} \\ &= -{R^c_{G,i}}^{-1} G^T_{2,i} P^c_{N+1} (F_i + \delta F_i) x_i - {R^c_{G,i}}^{-1} G^T_{2,i} P^c_{N+1} (G_{2,i} + \delta G_{2,i}) \\ &\quad \times u_{i-1} + {R^c_{G,i}}^{-1} G^T_{2,i} P^c_{N+1} G_{2,i} u_{i-1}. \end{aligned} \tag{B.5}$$

Considering the sampling period sufficiently small so that $x_i \approx x_{i-1}$, the (B.5) can be rewritten as

$$\begin{aligned} u_i &:= -{R^c_{G,i}}^{-1} G^T_{2,i} P^c_{N+1} ((F_i + \delta F_i) x_{i-1} + (G_{2,i} + \delta G_{2,i}) u_{i-1}) + {R^c_G}^{-1} \\ &\quad \times G^T_2 P^c_{N+1} G_{2,i} u_{i-1}. \end{aligned}$$

Hence, as $u_{i-1} = z_i$, the system (B.1) can be rewritten as system (7)–(8)

$$\begin{aligned} x_{i+1} &= (F_i + \delta F_i) x_i + (G_{2,i} + \delta G_{2,i}) u_i \\ \begin{bmatrix} \delta F_i & \delta G_i \end{bmatrix} &= H_i \Delta_i \begin{bmatrix} E_{F_i} & E_{G_i} \end{bmatrix}, \end{aligned}$$

where

$$u_i = -{R^c_{G,i}}^{-1} G^T_{2,i} P^c_{N+1} x_i + {R^c_{G,i}}^{-1} G^T_{2,i} P^c_{N+1} G_{2,i} z_i. \tag{B.6}$$

See details in Hassibi et al. (1999).

References

Alcala, E., Puig, V., Quevedo, J., Escobet, T., & Comasolivas, R. (2018). Autonomous vehicle control using a kinematic Lyapunov-based technique with LQR-LMI tuning. *Control Engineering Practice*, *73*, 1–12. http://dx.doi.org/10.1016/j.conengprac.2017.12.004, URL https://doi.org/10.1016/j.conengprac.2017.12.004.

Cerri, J. P., Terra, M. H., & Ishihara, J. Y. (2009). Recursive robust regulator for discrete-time state-space systems. In *2009 American control conference* (pp. 3077–3082). IEEE, http://dx.doi.org/10.1109/acc.2009.5160553, URL https://doi.org/10.1109/acc.2009.5160553.

Chu, Z., Sun, Y., Wu, C., & Sepehri, N. (2018). Active disturbance rejection control applied to automated steering for lane keeping in autonomous vehicles. *Control Engineering Practice*, *74*, 13–21. http://dx.doi.org/10.1016/j.conengprac.2018.02.002, URL https://doi.org/10.1016/j.conengprac.2018.02.002.

Dias, J. E. A., Pereira, G. A. S., & Palhares, R. M. (2014). Longitudinal model identification and velocity control of an autonomous Car. *IEEE Transactions on Intelligent Transportation Systems*, 1–11. http://dx.doi.org/10.1109/tits.2014.2341491, URL https://doi.org/10.1109/tits.2014.2341491.

Fagnant, D. J., & Kockelman, K. (2015). Preparing a nation for autonomous vehicles: opportunities, barriers and policy recommendations. *Transportation Research Part A: Policy and Practice*, *77*, 167–181. http://dx.doi.org/10.1016/j.tra.2015.04.003, URL https://doi.org/10.1016/j.tra.2015.04.003.

Fancher, P. S. (1989). Directional dynamics considerations for multi-articulated, multi-axled heavy vehicles. In *SAE technical paper series* (pp. 630–640). SAE International, http://dx.doi.org/10.4271/892499, URL https://doi.org/10.4271/892499.

Fu, M., Zhang, K., Yang, Y., Zhu, H., & Wang, M. (2015). Collision-free and kinematically feasible path planning along a reference path for autonomous vehicle. In *2015 IEEE intelligent vehicles symposium (IV)* (pp. 907–912). IEEE, http://dx.doi.org/10.1109/ivs.2015.7225800, URL https://doi.org/10.1109/ivs.2015.7225800.

Guan, H., Kim, K., & Wang, B. (2017). Comprehensive path and attitude control of articulated vehicles for varying vehicle conditions. *International Journal of Heavy Vehicle Systems*, *24*(1), 65. http://dx.doi.org/10.1504/ijhvs.2017.080961, URL https://doi.org/10.1504/ijhvs.2017.080961.

Hassibi, B., Sayed, A. H., & Kailath, T. (1999). *Indefinite-quadratic estimation and control*. Society for Industrial and Applied Mathematics, http://dx.doi.org/10.1137/1.9781611970760, URL https://doi.org/10.1137/1.9781611970760.

Houben, L. W. L. (2008). Analysis of truck steering behaviour using a multi-body model, Master's thesis, Eindhoven University of Technology, DCT 343.

Hu, C., Jing, H., Wang, R., Yan, F., & Chadli, M. (2016). Robust $\mathcal{H}_\infty$ output-feedback control for path following of autonomous ground vehicles. *Mechanical Systems and Signal Processing*, *70–71*, 414–427. http://dx.doi.org/10.1016/j.ymssp.2015.09.017, URL https://doi.org/10.1016/j.ymssp.2015.09.017.

Islam, M. M., Laine, L., & Jacobson, B. (2015). Improve safety by optimal steering control of a converter dolly using particle swarm optimization for low-speed maneuvers. In *2015 IEEE 18th international conference on intelligent transportation systems* (pp. 2370–2377). IEEE, http://dx.doi.org/10.1109/itsc.2015.383, URL https://doi.org/10.1109/itsc.2015.383.

Ji, X., He, X., Lv, C., Liu, Y., & Wu, J. (2018). Adaptive-neural-network-based robust lateral motion control for autonomous vehicle at driving limits. *Control Engineering Practice*, *76*, 41–53. http://dx.doi.org/10.1016/j.conengprac.2018.04.007, URL https://doi.org/10.1016/j.conengprac.2018.04.007.

Jujnovich, B. A., & Cebon, D. (2013). Path-following steering control for articulated vehicles. *Journal of Dynamic Systems, Measurement, and Control*, *135*(3), 031006. http://dx.doi.org/10.1115/1.4023396, URL https://doi.org/10.1115/1.4023396.

Kailath, T., Sayed, A. H., & Hassibi, B. (2000). *Linear estimation*. New Jersey: Prentice Hall.

Kati, M. S., Köroğlu, H., & Fredriksson, J. (2016). Robust lateral control of an A-double combination via $\mathcal{H}_\infty$ and generalized $\mathcal{H}_2$ static output feedback. *IFAC-PapersOnLine*, *49*(11), 305–311. http://dx.doi.org/10.1016/j.ifacol.2016.08.046, URL https://doi.org/10.1016/j.ifacol.2016.08.046.

Kim, K. -i., Guan, H., Wang, B., Guo, R., & Liang, F. (2016). Active steering control strategy for articulated vehicles. *Frontiers of Information Technology & Electronic Engineering*, [ISSN: 2095-9230] *17*(6), 576–586. http://dx.doi.org/10.1631/FITEE.1500211, URL https://doi.org/10.1631/FITEE.1500211.

Li, C., Jing, H., Wang, R., & Chen, N. (2018). Vehicle lateral motion regulation under unreliable communication links based on robust $\mathcal{H}_\infty$ output-feedback control schema. *Mechanical Systems and Signal Processing*, *104*, 171–187. http://dx.doi.org/10.1016/j.ymssp.2017.09.012, URL http://www.sciencedirect.com/science/article/pii/S0888327017304892.

Luijten, M. (2010). Lateral dynamic behaviour of articulated commercial vehicles, Master's thesis, Eindhoven University of Technology.

Massera Filho, C., Terra, M. H., & Wolf, D. F. (2017). Safe optimization of highway traffic with robust model predictive control-based cooperative adaptive cruise control. *IEEE Transactions on Intelligent Transportation Systems*, *18*(11), 3193–3203. http://dx.doi.org/10.1109/tits.2017.2679098, URL https://doi.org/10.1109/tits.2017.2679098.

Matraji, I., Al-Durra, A., Haryono, A., Al-Wahedi, K., & Abou-Khousa, M. (2018). Trajectory tracking control of skid-steered mobile robot based on adaptive second order sliding mode control. *Control Engineering Practice*, *72*, 167–176. http://dx.doi.org/10.1016/j.conengprac.2017.11.009, URL https://doi.org/10.1016/j.conengprac.2017.11.009.

Michałek, M. M. (2014). A highly scalable path-following controller for N-trailers with off-axle hitching. *Control Engineering Practice*, *29*, 61–73. http://dx.doi.org/10.1016/j.conengprac.2014.04.001, URL https://doi.org/10.1016/j.conengprac.2014.04.001.

van de Molengraft-Luijten, M. F., Besselink, I. J., Verschuren, R. M., & Nijmeijer, H. (2012). Analysis of the lateral dynamic behaviour of articulated commercial vehicles. *Vehicle System Dynamics*, *50*(sup1), 169–189. http://dx.doi.org/10.1080/00423114.2012.676650, URL https://doi.org/10.1080/00423114.2012.676650.

Nayl, T., Nikolakopoulos, G., Gustafsson, T., Kominiak, D., & Nyberg, R. (2018). Design and experimental evaluation of a novel sliding mode controller for an articulated vehicle. *Robotics and Autonomous Systems*, *103*, 213–221. http://dx.doi.org/10.1016/j.robot.2018.01.006, URL https://doi.org/10.1016/j.robot.2018.01.006.

Noorvand, H., Karnati, G., & Underwood, B. S. (2017). Autonomous vehicles. *Transportation Research Record: Journal of the Transportation Research Board*, *2640*, 21–28. http://dx.doi.org/10.3141/2640-03, URL https://doi.org/10.3141/2640-03.

Sayed, A. (2001). A framework for state-space estimation with uncertain models. *IEEE Transactions on Automatic Control*, *46*(7), 998–1013. http://dx.doi.org/10.1109/9.935054, URL https://doi.org/10.1109/9.935054.

Sayed, A. H., & Nascimento, V. H. (1999). Design criteria for uncertain models with structured and unstructured uncertainties. In *Robustness in identification and control* (pp. 159–173). Springer London, http://dx.doi.org/10.1007/bfb0109867, URL https://doi.org/10.1007/bfb0109867.

Scherer, C. (1995). Mixed h 2/h ∞ control. In *Trends in control* (pp. 173–216). Springer London, http://dx.doi.org/10.1007/978-1-4471-3061-1_8, URL https://doi.org/10.1007/978-1-4471-3061-1_8.

Schramm, D., Hiller, M., & Bardini, R. (2018). *Vehicle dynamics*. Springer Berlin Heidelberg, http://dx.doi.org/10.1007/978-3-662-54483-9, URL https://doi.org/10.1007/978-3-662-54483-9.

Shin, J., Huh, J., & Park, Y. (2015). Asymptotically stable path following for lateral motion of an unmanned ground vehicle. *Control Engineering Practice*, *40*, 102–112. http://dx.doi.org/10.1016/j.conengprac.2015.03.006, URL https://doi.org/10.1016/j.conengprac.2015.03.006.

Skjetne, R., & Fossen, T. (2001). Nonlinear maneuvering and control of ships. *3*, In *MTS/IEEE Oceans 2001. An ocean odyssey. Conference proceedings (IEEE Cat. No.01CH37295)* (pp. 1808–1815). Marine Technol. Soc, http://dx.doi.org/10.1109/oceans.2001.968121, URL https://doi.org/10.1109/oceans.2001.968121.

Terra, M. H., Cerri, J. P., & Ishihara, J. Y. (2014). Optimal robust linear quadratic regulator for systems subject to uncertainties. *IEEE Transactions on Automatic Control*, *59*(9), 2586–2591. http://dx.doi.org/10.1109/tac.2014.2309282, URL https://doi.org/10.1109/tac.2014.2309282.

Wu, N., Huang, W., Song, Z., Wu, X., Zhang, Q., & Yao, S. (2015). Adaptive dynamic preview control for autonomous vehicle trajectory following with DDP based path planner. In *2015 IEEE intelligent vehicles symposium (IV)* (pp. 1012–1017). IEEE, http://dx.doi.org/10.1109/ivs.2015.7225817, URL https://doi.org/10.1109/ivs.2015.7225817.

Yuan, H., & Zhu, H. (2016). Anti-jackknife reverse tracking control of articulated vehicles in the presence of actuator saturation. *Vehicle System Dynamics*, *54*(10), 1428–1447. http://dx.doi.org/10.1080/00423114.2016.1208251, URL https://doi.org/10.1080/00423114.2016.1208251.

Zhao, W., Zhang, H., & Li, Y. (2018). Displacement and force coupling control design for automotive active front steering system. *Mechanical Systems and Signal Processing*, *106*, 76–93. http://dx.doi.org/10.1016/j.ymssp.2017.12.037, URL http://www.sciencedirect.com/science/article/pii/S0888327017306751.